Journal of Korean Association of Crystal Growth
Vol. 9, No. 1 (1999) 1-5

Growth of $CaF_2:R^{3+}$ (R=Nd, Er) layers by molecular beam epitaxy

Jung Min Ko, Yefen Chen and Tsuguo Fukuda

Institute for Materials Research, Tohoku University, Sendai 980, Japan
(Received November 9, 1998)

Molecular beam epitaxy법에 의한 희토류 이온(Nd^{3+}, Er^{3+}) 첨가 CaF_2 박막의 성장

고정민, Yefen Chen, Tsuguo Fukuda

東北大學 金屬材料硏究所, 仙台市, 日本, 980-77
(1998년 11월 9일 접수)

Abstract The rare-earth ions (R^{3+}, R=Nd, Er) doped CaF_2 layers have been grown on CaF_2 (111) substrate by molecular beam epitaxy. The surface structure and the crystallinity of $CaF_2:R^{3+}$ layers depending on the doping concentration of R^{3+} and layer thickness were studied by reflection high-energy electron diffraction (RHEED). In aspect of application as buffer layer in semiconductor-related hybrid structure, the lattice displacement between $CaF_2:R^{3+}$ layers and CaF_2 (111) substrate was investigated by X-ray rocking curve analysis.

요 약 Molecular beam epitaxy법으로 CaF_2 (111) 기판위에 희토류 이온 (Nd^{3+}, Er^{3+}) 첨가 CaF_2 박막을 성장하였다. 첨가농도와 박막두께에 따른 희토류 첨가 CaF_2 박막의 표면구조와 결정성을 RHEED로 검토하였다. 반도체 관련 고집적회로구조에 있어서의 완충막으로서의 응용을 고려하여, 희토류첨가 CaF_2 바막과 CaF_2 (111) 기판과의 격자부정합의 변이를 X-ray rocking Curve 분석에 의해 검토하였다.

1. Introduction

For last several decades, the deposition of alkaline-earth fluorides (AF_2) such as CaF_2, SrF_2 and BaF_2 on a variety of semiconductors (Si, Ge, and GaAs) by MBE has been studied [1-7]. These fluorides were used as epitaxial buffers to grow semiconductor-insulator-semiconductor structures, which is a pre-requisite for long-ranged three dimensional integrated devices. Recently, the (Ca, Sr)F_2 or (Sr, Ba)F_2 solid solution films have been preferred because the mixture of these fluorides with different lattice constant (CaF_2=5.46 Å, SrF_2=5.80 Å, BaF_2=6.20 Å) are able to attain very close matching with basic semiconductor substrates (Si=5.43 Å, Ge=5.65 Å, GaAs=5.65 Å) or narrow gap IV-VI semiconductor materials (InP=5.87 Å, PbS=5.94 Å, PbSe=6.12 Å, PbTe=6.45 Å, CdTe=6.48 Å) [8-11]. Moreover, because the composition of the mixed fluoride buffer layer can be graded across its thickness, the superlattice structure having each interface good-matched between buffer layers and semiconductor layers.

The growth of rare-earth ion doped CaF_2 layers on the various substrates by MBE have been actively demonstrated for their photoluminescence study ($CaF_2:Nd^{3+}/CaF_2$ [12], $CaF_2:Nd^{3+}/Si$ [13], $CaF_2:Er^{3+}/CaF_2$ [14], $CaF_2:Er^{3+}/Si$ [15]). However, All of these reports have been done for only small amount of doping concentration less than 10 mol%, and have not shown the effect of rare-earth ions doping on the crystallinity and structure type of layers. To realize more useful semiconductor-related integrated circuitry, the growth of AF_2 layer doped by rare-earth ions (R^{3+}) of relatively large concentration should be studied sufficiently.

In this study, we reprot the MBE growth of R^{3+} (R=Nd, Er) doped CaF_2 layers on CaF_2 (111) subst rate, which was employed as the growing substance because CaF_2 is undoubtedly one of most popular buffer materials, and Nd and Er trivalent ions are very useful laser-active centers. The crystallinity and surface structure of $CaF_2:R^{3+}$ layers on CaF_2 (111) substrates depending on R^{3+} doping concentration

and layer thickness were studied by reflection high-energy electron diffraction (RHEED) pattern observation, and the lattice displacement between $CaF_2:R^{3+}$ layers and CaF_2 (111) substrate was investigated by X-ray rocking curve (XRC) analysis.

2. Experiments

The growth experiments were performed in a Eiko EL 10A MBE system equipped with conventional effusion cells containing boron nitride crucibles, in which powdered sources of CaF_2 and RF_3 (R=Nd, Er) respectively were charged and evaporated simultaneously. CaF_2 (111) substrates, 20×20 mm^2 and 1 mm thick, were degreased by trichloroethane, acetone, methanol and distilled water under ultrasonic bath in that order, and then were mounted on a molybdenum block in ultrahigh vacuum chamber. The protective oxide and contaminant layer were removed by heating the substrate at 650°C. Epitaxial growth was performed at substrate temperature of 600°C for $CaF_2:Nd^{3+}$ layers and 550°C for $CaF_2:Er^{3+}$ layers, which were optimal growth temperature for $Ca_{0.5}R_{0.5}F_{2.5}$ layer of stoichiometric composition in our preliminary experiments. The background pressure in the range of $\sim7.0\times10^{-8}$ torr was maintained throughout deposition. R^{3+} doping concentration was confirmed by electron probe microanalysis (EPMA). The overall thickness of $CaF_2:R^{3+}$ layers were determined by step profiler. The crystallinity, epitaxial relationship and the surface structures of $CaF_2:R^{3+}$ layers were studied in situ by RHEED patterns, which was shown at regular interval time by using electron beam gun of 15 keV energy. The layer thickness for each RHEED pattern was calculated through the data of the overall thickness of layer and growth time on the assumption that the growth rate is constant during overall deposition. The lattice displacement between $CaF_2:R^{3+}$ layers and CaF_2 (111) substrates was calculated by X-ray rocking curve (XRC) analysis for (111) reflection of CaF_2 substrate using a Philips XPert-MRD high-resolution diffractometer with Cu Kα radiation diffracted by four-crystal Ge (220) monochromator.

3. Result and discussion

For all $CaF_2:R^{3+}$ layers in the very initial growth stage, the sharp elongated streaky patterns with well-defined Kikuchi bands were obtained, which provided evidence of the good crystallinity of the $CaF_2:R^{3+}$ layer and the flatness of its surface on the atomic scale. Irrespective of doping concentration, all $CaF_2:Nd^{3+}$ layers and $CaF_2:Er^{3+}$ layers showed the six-fold periodicity feature that same RHEED patterns of layers should be shown from every rotation of substrate by 60°. This six-fold periodicity in RHEED pattern observation manifest that all $CaF_2:Nd^{3+}$ layers and $CaF_2:Er^{3+}$ layers up to 50 mol% doping concentration have hexagonal-type surface structure.

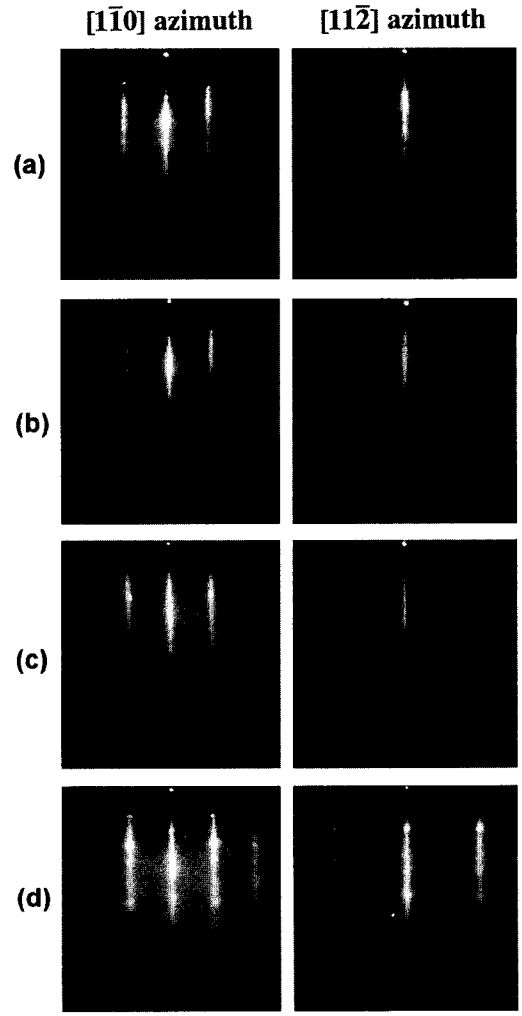

Fig. 1. RHEED patterns of (a) $CaF_2:Er^{3+}$ layer (~6000 Å, ~20 mol%), (b) $CaF_2:Nd^{3+}$ layer (~2200 Å, ~40 mol%), (c) $CaF_2:Er^{3+}$ layer (~2000 Å, ~45 mol%) and (d) $CaF_2:Er^{3+}$ layer (~4500 Å, ~45 mol%).

In Fig. 1, the notable RHEED patterns obtained from $CaF_2:R^{3+}/CaF_2$ (111) structure for $[1\bar{1}0]$ and $[11\bar{2}]$ azimuths of CaF_2 substrate are presented distinguishably, which show the layer crystallinity and surface structure corresponding to R^{3+} doping concentration and layer thickness. For the $CaF_2:Nd^{3+}$ layers (up to ~50 mol%) and the $CaF_2:Er^{3+}$ layers (up to ~40 mol%) the spacing between the streaks in both azimuths corresponds to electron diffraction from a surface with (1×1) structure which coincides with the structure of bulk CaF_2 crystals (Fig. 1(a) and (b)). Such simple RHEED pattern, (1×1), is characteristic of the surfaces of other alkaline-earth fluorides (SrF_2, BaF_2) [16, 17]. The $CaF_2:Nd^{3+}$ layers (<30 mol%) and the $CaF_2:Er^{3+}$ layers (<40 mol%) showed the sharp streaks patterns free of any remarkable spots or arcs even for their large thickness of ~6000 Å (Fig. 1(a)), which implicates that the Nd^{3+} or Er^{3+} trivalent ions in these doping range could be well incorporated into CaF_2 layer without changing its inherent fluorite structure or degrading significantly its crystallinity. However, the $CaF_2:Nd^{3+}$ layers of above ~30 mol% doping concentration begin to be gradually degraded showing the several weak arcs superimposed on streaks of (1×1) pattern when their thickness exceeds ~2000 Å (Fig. 1(b)). The presence of these arcs which were observed even from relatively thin and flat layer of ~2000 Å thickness (note that any tiny spots was not found in streaks) indicate that due to presumably the immiscibility of NdF_3 of tysonite structure and CaF_2 of fluorite structure, the layer became severely misoriented escaping early from the initial conformity to hexagonal arrangement of CaF_2 (111) surface atoms, thus, provided the grains of each isolated phase, which might be enhanced by the increase of layer thickness.

Figure 1(c) shows the RHEED patterns obtained for $[1\bar{1}0]$ and $[11\bar{2}]$ azimuths from $CaF_2:Er^{3+}$ layer with Er^{3+} doping concentration of 40 to 50 mol%. In this range containing stoichiometric composition, the RHEED patterns of $CaF_2:Er^{3+}$ layer have very remarkable additional feature that common (1×1) surface structure was replaced by (2×2) reconstructed surface structure in more than 200 Å thickness. This (2×2) surface reconstruction is characterized by the presence of fractional order streaks spaced by 1/2 of the main streak spacing on zeroth Laue zone in both azimuths (Fig. 1(c)). The well-defined (2×2) which was sustained showing sharp streaks, however, began to be degraded and was converted to spotty patterns together with weak arcs over ~4000 Å thickness (Fig. 1(d)). It is presumed that over this thickness the lattice relaxation by the formation and propagation of misfit dislocations, which provided the three-dimensional islands with rough flatness in atomic scale, was over-accumulated and exceedingly distorted, therefore, each phase of CaF_2 and ErF_3 could be enhanced to exist. However, it should be noted that the ErF_3 has more soluble with CaF_2 than NdF_3 does in epitaxial system.

Figure 2 shows reciprocal lattice set of the subcell and supercell corresponding to RHEED patterns of (1×1) and (2×2), which would explain schematically how their relationship should provide these RHEED patterns along the $[1\bar{1}0]$ and $[11\bar{2}]$ azimuth. Although the size of reciprocal unit cell should be dependent on the species of dopants and its concentration, it did not be considered in Fig. 2. In fact, for the RHEED patterns observed corresponding several doping concentration range, the spacing of streaks diffracted from subcell lattice was negligibly equivalent to each other. In Fig. 3, the dependency of $CaF_2:R^{3+}$ (R=Nd, Er)/CaF_2 (111) surface structure on R^{3+} doping concentration and layer thickness described avove, is summarized, where the value of thickness in each isolated area was approximated to be constant even though in fact it might vary with doping concentration.

The lattice displacement between $CaF_2:R^{3+}$ layer and CaF_2 (111) substrate along the [111] growth direction was calculated from angular difference ($\Delta\theta$) of X-ray rocking curves for (111) reflection between layer and substrate. On the assumption that all $CaF_2:R^{3+}$ layers has the fluorite structure,

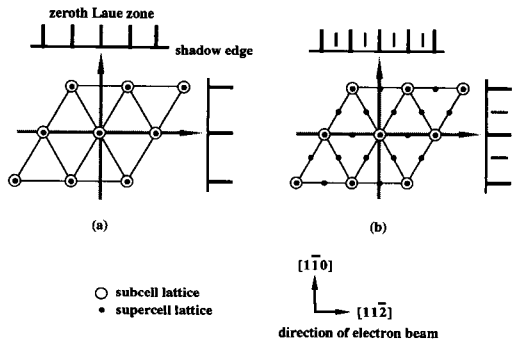

Fig. 2. The reciprocal lattice sections corresponding to RHEED patterns of $CaF_2:R^{3+}$ (R=Nd, Er) layers: (a) (1×1) and (b) (2×2) surface structure.

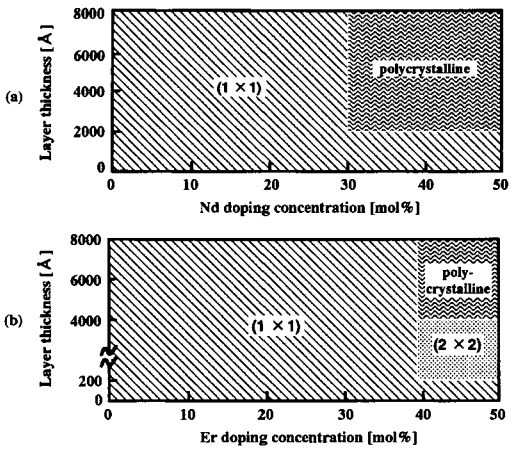

Fig. 3. The map showing the transition of RHEED pattern of (a) $CaF_2:Nd^{3+}$ layers and (b) $CaF_2:Er^{3+}$ layers corresponding to Nd or Er doping concentration and layer thickness.

their lattice constants was derived from the data of a_{CaF2}=5.46295 Å [18] and lattice displacements of [111] direction, and compared with those of several semiconductor materials (Fig. 4). In the range over ~40 mol% there is a large deviation from proximate line of lattice displacement, which seems to be attributed probably to degradation of layer crystallinity in this range proved by observation of RHEED pattern. Nevertheless, this result of X-ray rocking curve analysis for (111) reflection is characterized by the linearity that the lattice constant of $CaF_2:R^{3+}$ layers increases continuously depending on R^{3+} doping concentration. The increment of lattice constant of $CaF_2:Nd^{3+}$ and $CaF_2:Er^{3+}$

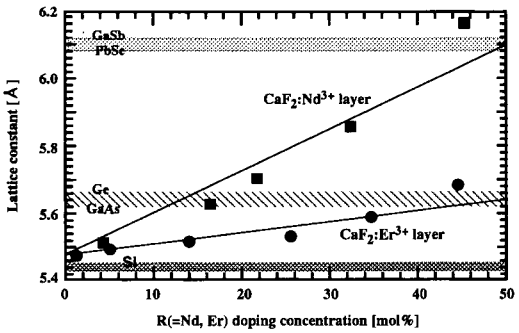

Fig. 4. Lattice constants of $CaF_2:R^{3+}$ (R=Nd, Er) layers depending on doping concentration (lattice constants of several semiconductors are designated as thick horizontal lines for comparison with those of $CaF_2:R^{3+}$ layers).

layer corresponding to 1 mol% incorporation of Nd^{3+} and Er^{3+} is estimated to be 0.0124 Å and 0.0033 Å respectively, which allows for $CaF_2:Nd^{3+}$ layer and $CaF_2:Er^{3+}$ layer to well-match selectively with various semiconductor materials as buffer layer.

4. Summary

The $CaF_2:R^{3+}$ (R=Nd, Er) layers up to ~50 mol% doping concentration have been grown on CaF_2 (111) substrate by molecular beam epitaxy. By the observation of RHEED pattern, it was known that the $CaF_2:Nd^{3+}$ layers have only (1×1) surface structure and $CaF_2:Er^{3+}$ layers have (1×1) and (2×2) surface structure. ErF_3 could be well incorporated with CaF_2 providing $CaF_2:Er^{3+}$ layers of good monocrystallinity up to ~4000 Å layer thickness, whereas the incorporation of NdF_3 above ~30 mol% to CaF_2 degraded the crystallinity of $CaF_2:Nd^{3+}$ layers in more than ~2000 Å thickness due to immiscibility of each other. The lattice constant of $CaF_2:Nd^{3+}$ and $CaF_2:Er^{3+}$ layers increased linearly depending on doping concentration of Nd^{3+} and Er^{3+}, which could propose the availability as buffer layer well-matching selectively with various semiconductor.

References

[1] T. Asano and H. Ishiwara, J. Appl. Phys. 55 (1984) 3566.
[2] T.P. Smith III, J.M. Phillips, W.M. Augustyniak and P.J. Stiles, Appl. Phys. Lett. 45 (1984) 907.
[3] S. Sinharoy, R.A. Hoffman, J.H. Rieger, R.F.C. Farrow and A.J. Noreika, J. Vac. Sci. Technol. A3 (1985) 842.
[4] J.M. Phillips, L.C. Feldman, J.M. Gibson and M. L. McDonald, Thin Solid Films 107 (1983) 217.
[5] L.J. Schowalter and R.M. Fathauer, J. Vac. Sci. Technol. A4 (1986) 1026.
[6] S. Siskos, C. Fontaine and A. Munoz-Yague, Appl. Phys. Lett. 44 (1984) 1146.
[7] H. Zogg and M. Hüppi, Appl. Phys. Lett. 47 (1985) 133.
[8] A.N. Tiwari, W. Floeder, S. Blunier, H. Zogg and H. Weibel, Appl. Phys. Lett. 57 (1990) 1108.
[9] B. Schumann, G. Kühn, W. Gasch, G. Wagner, R. Flagmeyer, O. Müller and W. Hauffe, J. Crystal Growth 82 (1987) 405.
[10] C.W. Tu, T.T. Sheng, A.T. Macrander, J.M. Phillips and H.J. Guggenheim, J. Vac. Sci. Technol.

B2(1) (1984) 24.
[11] K. Tsutsui, H. Ishiwara, T. Asano and S. Furukawa, Appl. Phys. Lett 46 (1985) 1131.
[12] L.E. Bausa, R. Legros and A. Munoz-Yague, Appl. Phys. Lett. 59 (1991) 152.
[13] C.C. Cho, W.M. Duncan, T.H. Lin and S.K. Fan, Appl. Phys. Lett. 61 (1992) 1757.
[14] E. Daran, R. Legros, A. Munoz-Yague, C. Fontaine and L.E. Bausa, J. Appl Phys. 75 (1994) 2749.
[15] L.E. Bausa, C. Fontaine, E. Daran and A. Munoz-Yague, J. Appl. Phys. 72 (1992) 499.
[16] K. Sugiyama, J. Appl. Phys. 56 (1984) 1733.
[17] H. Zogg, S. Blunier and J. Masek, J. Electrochem. Soc. 136 (1989) 775.
[18] R.W.G. Wyckoff, Crystal Structure, Vol. 1, 2nd ed., (1982) p. 241.